Visual responses in the dorsal Lateral Geniculate Nucleus (dLGN) at early stages of retinal degeneration in *rd*[1]PDE6β mice

Running title: Visual responses in the dLGN during early stage retinal degeneration

Authors: Christopher A. Procyk

Annette E. Allen

Franck P. Martial

Robert J. Lucas

All work was conducted at the University of Manchester in R.J. Lucas' laboratory:

AV Hill Building
Faculty of Biology, Medicine and Health
University of Manchester
Oxford Road
Manchester
M13 9PT
United Kingdom

Corresponding Author:

R. J. Lucas

AV Hill Building
Faculty of Biology, Medicine and Health
University of Manchester
Oxford Road
Manchester
M13 9PT
United Kingdom

E-mail: robert.lucas@manchester.ac.uk

Telephone: +44 161 275 5251

Abstract

Inherited retinal degenerations encompass a wide range of diseases that result in the death of rod and cone photoreceptors eventually leading to irreversible blindness. Low vision survives at early stages of degeneration, at which point it could rely on residual populations of rod/cone photoreceptors as well as the inner retinal photoreceptor, melanopsin. To date, the impact of partial retinal degeneration on visual responses in the primary visual thalamus (dorsal lateral geniculate nucleus; dLGN) remains unknown, as does their relative reliance upon surviving rods and cone photoreceptors versus melanopsin. To answer these questions, we record visually evoked responses in the dLGN of anaesthetised *rd*^{1} mice using in-*vivo* electrophysiology at an age (3-5 weeks) at which cones are partially degenerate and rods are absent. We found that excitatory (ON) responses to light had lower amplitude and longer latency in *rd*^{1} compared to age-matched visually intact controls; however, contrast sensitivity and spatial receptive field size were largely unaffected at this early stage of degeneration. Responses were retained when those wavelengths to which melanopsin is most sensitive were depleted, indicating that they were driven primarily by surviving cones. Inhibitory responses appeared absent in the *rd*^{1} thalamus, as did light-evoked gamma oscillations in firing. This description of fundamental features of the dLGN visual response at this intermediate stage of retinal degeneration provide a context for emerging attempts to restore vision by introducing ectopic photoreception to the degenerate retina.

Keywords: *Retinal degeneration, dorsal Lateral Geniculate Nucleus (dLGN), Cone photoreceptor, Melanopsin, spatial receptive field, receptor substitution.*

55 **New and Noteworthy**

56

57 This study provides new therapeutically relevant insights to visual responses in the dorsal Lateral
58 Geniculate Nucleus (dLGN) during progressive retinal degeneration. Using in-*vivo* electrophysiology,
59 we demonstrate that visual responses have lower amplitude and longer latency during
60 degeneration, but contrast sensitivity and spatial receptive fields remain unaffected. Such visual
61 responses are driven predominantly by surviving cones rather than melanopsin photoreceptors. The
62 functional integrity of this visual pathway is encouraging for emerging attempts at visual restoration.

63

64

65 **Introduction**

66 Inherited retinal degenerations, such as retinitis pigmentosa, are the most common cause of
67 blindness in humans with an incidence of 1:4000. Irrespective of aetiology, most affect the outer
68 retina and lead to progressive and irreversible death of rod and cone photoreceptors at advanced
69 stages of the disease. In the *rd*[1] mouse model of retinitis pigmentosa, the retina undergoes well-
70 defined stages of cell death and re-organisation (Strettoi, Pignatelli et al. 2003, Jones and Marc
71 2005). Rod photoreceptors die rapidly to be lost by post-natal day 18 (P18) (Greferath, Goh et al.
72 2009) and this is followed by progressive degeneration of the cone photoreceptor population (Lin,
73 Masland et al. 2009) and remodelling of the inner retinal neurones (Strettoi and Pignatelli 2000,
74 Strettoi, Porciatti et al. 2002, Marc, Jones et al. 2003). However, isolated pockets of cones can
75 survive into the later stages of the disease (Carterdawson and Lavail 1979, Jimenez, GarciaFernandez
76 et al. 1996, Ogilvie, Tenkova et al. 1997) mirroring some human conditions.

77 The anatomical changes in the retina are mirrored by changes in the electrophysiological properties
78 of residual light-responses and the retinal network. During partial degeneration, residual light-
79 responses recorded from retinal ganglion cells already show a reduction in response amplitude and
80 slower signalling kinetics (Strettoi, Porciatti et al. 2002, Stasheff 2008, Gibson, Fletcher et al. 2013).
81 As a consequence of photoreceptor degeneration and remodelling, the remaining inner retinal
82 neurones exhibit robust rhythmic oscillations (Menzler and Zeck 2011, Choi, Zhang et al. 2014) and
83 an increase in baseline firing at rest (Stasheff 2008). A third source of light responses (the
84 photopigment melanopsin expressed in a specialised subset of retinal ganglion cells; RGCs) is less
85 impacted by degeneration. These cells survive retinal degeneration in adults with broadly normal
86 retinal anatomy (Vugler, Semo et al. 2008, Lin and Peng 2013) and drive excitatory responses to light
87 in various brain regions including the dorsal Lateral Geniculate Nucleus (dLGN) (Brown, Gias et al.
88 2010, Procyk, Eleftheriou et al. 2015).

Little is known about central responses to visual stimuli in progressive retinal degeneration. In advanced stages, responses in the visual thalamus originate solely from melanopsin and have extremely poor spatio-temporal resolution (Brown, Gias et al. 2010, Procyk, Eleftheriou et al. 2015). In this condition, spatial receptive fields for the melanopsin response of individual dLGN units can be very large, and melanopsin-driven responses to simple light steps dissipate over tens of seconds (Procyk, Eleftheriou et al. 2015). It remains unclear how disrupted visual responses are at earlier stages of degeneration, nor the extent to which these responses rely upon melanopsin versus surviving cones. Here we address this unknown by recording visual responses in the dLGN of juvenile *rd*^{1} mice at an age at which significant numbers of cone photoreceptors survive but rods are absent. We find a variety of light-responsive units throughout the dLGN of juvenile *rd*^{1} mice that exhibit low amplitude and enhanced latency (as previously reported for retinal responses in such animals). Contrast sensitivity was however retained, and the spatial receptive fields of dLGN units in this model were at least as fine as those of wild type mice. Application of the principles of silent substitution to bias stimuli against stimulating melanopsin indicated that dLGN light responses were driven primarily by surviving cones.

105 **Methods**

106

107 **Ethical Approval**

108 The care and use of all mice in this study was carried out in strict accordance with UK Home Office
109 regulations, UK Animals (Scientific Procedures) Act of 1986 (revised in 2012) and approved by the
110 local Manchester Animal Welfare and Ethical Review Board (AWERB reference 50/02506). All in-*vivo*
111 surgical procedures were performed under terminal urethane anaesthesia and all efforts were made
112 to minimise suffering.

113 **Animals**

114 Mice were bred at the University of Manchester and housed under a 12:12 light/dark cycle, with
115 food and water available *ad libitum*. As we aimed to use the method of receptor silent substitution
116 to separate cone from melanopsin evoked responses we undertook experiments on *Opn1mw*^{R} mice
117 (Stock Number: 008619; Jackson Laboratories) in which a coding sequence for the human long
118 wavelength sensitive cone opsin is knocked into the medium wavelength sensitive cone opsin locus.
119 These animals have a fully functional visual system but have enhanced divergence in spectral
120 sensitivity between cones and melanopsin allowing for the use of carefully designed stimuli to
121 dissect the contribution of individual photoreceptors to the light-response. Our colony of *Opn1mw*^{R}
122 mice has been backcrossed to the C57BL/6J mouse line for >9 generations. *Opn1mw*^{R} mice
123 homozygous for the *rd*^{1} mutation (*PDE6B*$^{rd1/rd1}$) were created in house by crossing this established
124 colony of *Opn1mw*^{R} mice with commercially available C57 *rd*^{1} mice (Stock Number: 004766; Jackson
125 Laboratories). Note that *Opn1mw*^{R} refers to the transgenic allele originally generated by (Smallwood,
126 Olveczky et al. 2003), and termed simply 'R' by them. For all electrophysiological experiments,
127 *Opn1mw*^{R} and *rd*^{1} *Opn1mw*^{R} were used between 3 - 5 weeks of age.

128 **In-*vivo* electrophysiology**

129 Six juvenile C57 *rd/rd Opn1mw*^{R} mice and eight juvenile *Opn1mw*^{R} were administered with 20%
130 Urethane (1.6mg/kg; i.p.). Once anaesthetised, mice were mounted onto a bespoke stereotaxic
131 frame (SG-4N-S, Narishige, Japan) which was fixed onto a 'lazy Susan' (RBB12A; Thorlabs, Germany).
132 Core body temperature was maintained at 37°C with a homeothermic blanket (Harvard Apparatus;
133 Kent, UK). An incision to expose the skull surface was made and a small hole (~1 mm diameter) was
134 drilled 2.2 mm posterior and 2.2 mm lateral to the bregma, targeting the dorsal LGN. A recording
135 probe (A4X8-5 mm-50-200-413; Neuronexus, MI, USA) consisting of four shanks (spaced 200µm
136 apart), each with eight recordings sites (spaced 50µm apart), was then positioned centrally on the
137 exposed surface in the coronal plane, and lowered to a depth of 2.5 - 3.3mm to target the dorsal
138 LGN using a fluid filled micromanipulator (MO-10; Narishige, Japan). Once the recording probe was
139 in position, mice were dark adapted for 30 minutes in order to allow neuronal activity to stabilise
140 following probe insertion. Stimuli were presented to the eye contralateral to the craniotomy, which
141 was treated with topical atropine sulphate (1% w/v; Sigma- Aldrich, UK) to dilate the pupil and
142 mineral oil to keep the cornea moist. The ipsilateral eye remained covered with blackout material
143 throughout the entire experiment. In some experiments, following recording in one location the
144 probe was moved 200µm caudal and a second set of responses recorded. Neural signals were
145 acquired using a Recorder64 system (Plexon Inc; TX, USA). Signals were amplified x3000, high-pass
146 filtered at 300 Hz and digitized at 40 kHz. Multiunit activity (spikes with amplitudes >50µV) were
147 saved as time-stamped waveforms and analysed offline (see data analysis).

148 **Presentation of visual stimuli**

149 Light stimuli were generated in MATLAB (The Mathworks Inc.; MA, USA) and controlled by a laptop
150 running PsychoPy V2.6 (Peirce 2008). Light stimuli were presented via a commercially available

151 projection system which had been modified so that each of the Red, Green and Blue channels was a
152 combination of up to five independently controlled wavelengths (λ_{max} = 405, 455, 525, 561, 630nm)
153 as previously described (Allen, Storchi et al. 2017). This allowed us to present patterned stimuli that
154 only present spatial/temporal contrast for particular photopigments in our *Opn1mw*^{R} and *rd*^{1}
155 *Opn1mw*^{R} mice (Figure 1A). As such we designed three multispectral stimuli allowing the
156 contribution of cone opsin and melanopsin to the *rd*^{1} light response to be defined using receptor
157 silent substitution (Figure 1B). Transition from spectrum 1 (green trace) to spectrum 3 (orange trace)
158 was designed to provide a positive contrast for all photoreceptors in the *Opn1mw*^{R} retina ('All
159 photoreceptor' stimulus S-Cone: 51%; L-Cone: 47%; Rod: 34% and Melanopsin: 51%). This was
160 matched with a 'mel-less' stimulus (transition from spectrum 2 (pink trace) to Spectrum 3 (orange
161 trace)) providing equivalent contrast for S-Cones (50%), L-Cone (49%) and Rods (30%), but very low
162 contrast for melanopsin (< 5%). A full table of the effective irradiance change and Michelson contrast
163 for each photopigment during spectral transitions is shown in Figure 1C. All light measurements
164 were measured using a calibrated spectroradiometer (SpectroCal; Cambridge Research Instruments,
165 UK). Effective photon flux for each photopigment was determined using the calculated spectra and
166 visual pigment template described by (Govardovskii, Fyhrquist et al. 2000). The projector screen was
167 positioned in the centre of the visual field relative to the eye contralateral to the recording probe so
168 that the horizontal and vertical meridians of the stimulus display subtended 72° in azimuth and 57°
169 in elevation, respectively. To confirm these calibrated stimuli indeed had the expected
170 photopigment selectivity, we presented 50 repeats of full field "all photoreceptor" and "mel-less"
171 flashes at the beginning of each recording at a frequency of 4Hz. As expected, visual responses to
172 "all photoreceptor" and "mel-less" stimuli were equivalent under these conditions in both visually
173 intact (Figure 1D) and degenerate mice (Figure 1E). We characterised the responses of these units to
174 our "all photoreceptor" and "mel-less" conditions by quantifying (F) the peak response amplitude
175 and (G) the latency to peak response in both *Opn1mw*^{R} and *rd*^{1} *Opn1mw*^{R} mice. We found there to

176 be no significant differences between the two stimulus conditions for amplitude (*Opn1mw*^{R}*;* p = 0.09
177 and *rd*^{1} *Opn1mw*^{R}*;* p = 0.79) or latency (*Opn1mw*^{R}; p = 0.97 and *rd*^{1} *Opn1mw*^{R}; p = 0.27).

178 **Visual Stimuli**

179 *Dark-adapted responses:* At the beginning of each experiment we presented 200ms full field flashes
180 (irradiance = 2.50x10^{14} photons cm^{-2} s^{-1}) from darkness with a 1 second inter-stimulus interval (ISI)
181 for 50 repeats. We additionally presented 10s light-steps from darkness to the same irradiance with
182 an ISI of 50 second over 20 repeats to identify those units which possessed a sustained component
183 to the light-response.

184 *Contrast sensitivity*: Full field 1s light-steps, with a 5 second inter stimulus interval, were presented
185 at eight increasing cone contrasts (1%, 2%, 5%, 16%, 20%, 30%, 40% and 50%) from a light adapted
186 background (irradiance = 2.64x10^{14} photons cm^{-2} s^{-1}). Each sequence was repeated 20 times in an
187 interleaved manner using the "all-photoreceptor" stimulus settings described above.

188 *Receptive field mapping*: Vertical bars (occupying ~13° of the visual field; irradiance = 1.04x10^{14}
189 photons cm^{-2} s^{-1}) from a background (irradiance = 1.55x10^{13} photons cm^{-2} s^{-1}) were used to map
190 receptive fields of dLGN neurons using the "all photoreceptor" stimulus condition. Vertical bars were
191 presented for 250ms in a pseudorandom order in 13 (overlapping) spatial locations (4.5° separation
192 in bar position; ISI = 1.25 seconds). The spectra used for these spatial stimuli did not elicit significant
193 responses in the *rd*^{1} population. However, as these mice do not possess functional rods, we were
194 able to generate a new spectral transition which allowed us to present bars with a larger calculated
195 Michaelson contrast for both S- and L-cone opsins. Spatial receptive fields for *rd*^{1} mice were mapped
196 under these new settings.

197 *Silent Substitution Steps*: We initially presented full field transitions (4Hz) between our two pairs of
198 silent substitution stimuli: “all-photoreceptor” and “mel-less”. The stimulus spectra were adjusted
199 every 50 repeats in order to validate the stimulus conditions. Following this, full field 10s light steps
200 from a light adapted background were presented 20 times with a 50 second inter-stimulus interval
201 under the “all-photoreceptor” and “mel-less” stimulus conditions. Stimuli were presented in a
202 pseudorandom order in order to determine the contribution of activating both cones and
203 melanopsin together and cones in isolation.

204 **Data Analysis & Statistics**

205 Offline, neural waveforms were processed using Offline Sorter (version 2.8.8; Plexon Inc. USA).
206 Cross-channel artefacts were identified and removed, and then each channel analysed separately.
207 For each channel, single-unit spikes were detected and categorised based on the spike waveform via
208 a principal component analysis, whereby distinct clusters of spikes were readily identifiable and
209 showed a clear refractory period in their interspike interval distribution (>1ms). Single unit data
210 were subsequently sent to NeuroExplorer (version 4.032; Nex Technologies, MA, USA) and MATLAB
211 R2010a (The Mathworks Inc.) to further analyse changes in firing rate of single units in response to
212 the different visual stimuli presented. Statistical analysis and figure generation were conducted in
213 Graphpad Prism 7 and Corel Draw, respectively.

214 *Identification of light responses*: In the dark-adapted state, single units were classed as light
215 responsive if the firing rate during stimulus presentation exceeded 2 standard deviations of the
216 mean baseline firing rate prior to light exposure. Presentation or the 10s light-step under the dark-
217 adapted state allowed us to qualitatively categorise cells based on their light-response profile.
218 Accordingly, single units were defined as Transient ON if they demonstrated significant change in
219 firing rate after light onset which quickly returned to baseline during the light pulse. Transient ON-

220 OFF cells also showed an initial increase in firing rate at light onset before quickly returning to
221 baseline, however showed a second significant increase in firing immediately after light-offset.
222 Sustained-ON and Sustained-OFF cells were categorised if a significant increase or decrease in firing
223 rate was maintained for more than 5 seconds of a 10 second light-step, respectively. Under light-
224 adapted conditions, single units were categorised based on their response to the "all-
225 photoreceptor" condition.

226 *Contrast Sensitivity Analysis*: Single units were filtered to ensure that the firing rate at the maximum
227 cone contrast (50%) demonstrated a significant change in firing rate which was >2 standard
228 deviations above the pre-stimulus baseline. If this criterion was met, the response of that unit at the
229 seven lower contrasts was used for analysis regardless of whether it crossed the confidence interval.
230 Contrast sensitivity curves were calculated by subtracting the pre-stimulus baseline from the
231 average firing rate over the first 500ms of the 1 second light step. Sensitivity curves were compared
232 with an F-test in Graphpad Prism 7 (GraphPad software Inc.), to test whether the sensitivity of visual
233 responses in each genotype were best fit with a single, or two individual, curves. For population
234 data, we fitted a normalised dose-response function to individual units from Opn1mw^{r} and rd^{1}
235 Opn1mw^{r} mice and compared the cone contrast at half maximum response (for units with an R^2>0.6)
236 using an unpaired t-test.

237 *Spatial Receptive field analysis*: To qualify for inclusion in our assessment of receptive field size,
238 single units had to show a significant change in firing rate (>2SD above baseline) to at least one bar
239 position over 90 repeats of the stimulus sequence. The spatial receptive field size for single units
240 meeting this criterion was estimated by fitting a 2-Dimensional Gaussian fit (R^2 > 0.7) to the
241 relationship between response amplitude and bar position in Graphpad Prism 7 (GraphPad software
242 Inc.). The receptive field size for individual cells was described as 1 standard deviation of the best-fit
243 Gaussian.

244 *Silent Substitution Analysis*: Single units were first classified as sustained or transient based on their
245 response to a 10s light-step under the "all photoreceptor" condition. Single units were classified as
246 sustained if they maintained their change in firing rate greater than two standard deviations above
247 baseline for more than 5s over the course of the 10s light step. Comparisons between the total
248 number of spikes (calculated by integrating under the PSTH from 2-10s during light-exposure) in the
249 "all photoreceptor" and "mel-less" conditions in both genotypes was used to determine the
250 contribution of melanopsin signalling to the dLGN and were analysed using 2-Way ANOVA (with post
251 hoc Bonferroni correction) in Graphpad Prism 7 (GraphPad software Inc.).

252 **Tissue Preparation**

253 Following electrophysiological recordings, mice were transcardially perfused with 0.9% saline
254 followed by cold 4% methanol-free paraformaldehyde (Sigma Aldrich; UK). The brain was removed
255 and post-fixed overnight in 4% paraformaldehyde, prior to cryoprotection for 24 hours in 30%
256 sucrose in 0.1M PBS. 100µm coronal sections were cut using a sledge microtome, mounted onto
257 glass slides and cover slips were applied using Vectashield (Vector Laboratories, Inc.). Electrode
258 placement in the dLGN was confirmed by visualisation of a fluorescence dye (Cell Tracker CM-DiI;
259 Invitrogen Ltd. Paisley, UK) applied to the probe prior to recording and compared to the stereotaxic
260 mouse atlas. Images were collected on an Olympus BX51 upright microscope using a 4x/ 0.30 Plan
261 Fln, and captured using a Coolsnap ES camera (Photometrics) through MetaVue Software (Molecular
262 Devices). Specific band pass filters set for DAPI, FITC and Texas red prevented bleed through of
263 channels.

264 **Results**

265 We set out to describe the impact of partial retinal degeneration on dLGN visual responses using
266 young *rd*^{1} in which loss of cones is incomplete. In order to facilitate attempts to determine whether
267 surviving responses originated with cones or the inner retinal photoreceptor, melanopsin, we used
268 animals further manipulated to shift the spectral sensitivity of cones expressing medium wavelength
269 sensitive opsin to longer wavelengths far from those favoured by melanopsin (*Opn1mw*^{R};
270 (Smallwood, Olveczky et al. 2003)). We first presented full field 200ms flashes (2.50x10^{14} photons
271 cm^{-2} s^{-1}) from darkness to eight *Opn1mw*^{R} and six *rd*^{1} *Opn1mw*^{R} mice (3-5 weeks of age) and recorded
272 responses in the dLGN using extracellular multi-channel recording electrodes. Light-evoked changes
273 in activity were recorded across the anatomical extent of the dLGN in *rd*^{1} *Opn1mw*^{R} mice (shown for
274 a representative individual in Figures 2A&B). Although we could detect visual responses in all
275 animals, we found the number of light-responsive units per electrode placement to be negatively
276 correlated with age in the *rd*^{1} *Opn1mw*^{R} (black crosses; linear regression slope = -1.35; p = 0.003) but
277 not visually intact animals (green crosses; linear regression slope = 0.67; p>0.05; Figure 2C).

278 We next presented 10s full field pulses from darkness (irradiance = 2.50x10^{14} photons cm^{-2} s^{-1}) and
279 could categorise light-responsive units into four qualitatively distinct groups: transient ON, transient
280 ON-OFF, sustained ON and sustained OFF. Transient-ON units show an initial increase in firing rate at
281 light onset but quickly return to baseline (Figure 2D; top row). Transient ON-OFF units show a
282 transient increase in firing at both light onset and offset (Figure 2D; second row). Sustained ON units
283 demonstrate an initial increase in firing rate at light onset and firing remained elevated above
284 baseline throughout the duration of the light stimulus (Figure 2D; third row). Conversely, sustained
285 OFF units show a reduction in firing rate maintained over the duration of the light stimulus (Figure
286 2D; bottom row). In visually intact *Opn1mw*^{R} mice of equivalent age 24% of light-responsive units
287 were transient-ON; 23% transient ON-OFF; 45% sustained-ON; and 8% sustained-OFF. Light-

288 responses in *rd*^{1} *Opn1mw*^{R} mice were more transient in nature, with 65% of light-responsive units
289 having a transient ON; 15% a transient ON-OFF; and only 20% a sustained ON response. We did not
290 find a single example of a sustained OFF responses in the *rd*^{1} *Opn1mw*^{R} population.

291 We then set out to characterise the transient ON component of these visual responses. We found
292 that there was a significant difference in the peak response amplitude of light responses when
293 comparing transient units in *Opn1mw*^{R} mice and *rd*^{1} *Opn1mw*^{R} (Figure 2E; mean±SEM ΔFR = 9.07 ±
294 0.44 Spikes/s and 6.21 ± 0.53 Spikes/s, respectively; p = 0.026; 2-way ANOVA with post hoc
295 Bonferroni correction). Sustained units in *Opn1mw*^{R} mice also exhibited larger amplitude responses
296 compared to transient units in *rd*^{1} *Opn1mw*^{R} mice (mean±SEM ΔFR = 10.45 ± 0.9 Spikes/s and 6.21 ±
297 0.53 Spikes/s, respectively; p = 0.0002; 2-way ANOVA with post hoc Bonferroni correction).
298 Sustained units in the *rd*^{1} *Opn1mw*^{R} mice (mean±SEM ΔFR = 9.70 ± 1.56 Spikes/s) were not
299 significantly different to transient units (p>0.99) or sustained units (p>0.99) in *Opn1mw*^{R} mice.
300 Response latency was also significantly increased for units in *rd*^{1} *Opn1mw*^{R} mice compared to
301 *Opn1mw*^{R} mice (Figure 2F; p = <0.0001). Latency was calculated for transient and sustained
302 populations separately and showed that the time to peak response was significantly increased for
303 transient units in *rd*^{1} *Opn1mw*^{R} mice compared to *Opn1mw*^{R} mice (mean±SEM = 208.6 ± 5.25ms and
304 153.6 ± 6.27ms, respectively; p = <0.0001; 2-way ANOVA with post hoc Bonferroni correction) but
305 not for sustained units (mean±SEM = 168.2 ± 10.50ms and 202.4 ± 9.21ms, respectively; p = 0.20; 2-
306 way ANOVA with post hoc Bonferroni correction). Sustained units in *Opn1mw*^{R} mice also showed
307 significantly faster responses (mean±SEM = 168.2 ± 10.50ms) compared to transient units in *rd*^{1}
308 *Opn1mw*^{R} mice (mean±SEM = 208.6 ± 5.25ms; p = 0.0009; 2-way ANOVA with post hoc Bonferroni
309 correction). Turning our attention to the sustained component of visual responses, we calculated the
310 strength of the sustained response in both *Opn1mw*^{R} and *rd*^{1} *Opn1mw*^{R} mice by integrating under
311 the PSTH from the end of the transient increase in firing to the end of the light pulse (0.25s-10s).
312 Here we found that the total number of spikes was significantly greater for sustained units in the

313 *Opn1mw*^{R} dLGN (mean±SEM Total Spikes = 112.1 ± 14.52 Spikes) compared to the *rd*^{1} *Opn1mw*^{R}
314 dLGN (mean±SEM Total Spikes 20.36 ± 3.28 Spikes; Figure 2G; p = 0.0028; unpaired T-test).
315 Irradiance steps induce narrow band oscillations in the mouse dLGN (Saleem, Lien et al. 2017,
316 Storchi, Bedford et al. 2017). Power spectrum density analysis of firing rates upon presentation of
317 these 10s light steps revealed such behaviour (a robust oscillation at 31.3 ± 0.39Hz; Figure 2H) in
318 *Opn1mw*^{R} mice (green trace) but not in *rd*^{1} *Opn1mw*^{R} mice (black trace).

319 We next sought to characterise the sensory capabilities of juvenile *rd*^{1} *Opn1mw*^{R} mice in more detail.
320 For this purpose, we used the approach of receptor silent substitution to separately interrogate
321 responses driven by cones vs. melanopsin under light-adapted conditions (see Figure 1 in methods
322 for stimuli descriptions). Concentrating first on cone-driven responses, we presented 1 second light
323 steps from a light-adapted background (irradiance = 2.64×10^{14} photons cm^{-2} s^{-1}) with cone contrasts
324 ranging from 1 - 50%, but with minimal predicted melanopsin contrast. We identified 61 units that
325 showed a significant change in firing rate following light onset at the highest contrast in the
326 *Opn1mw*^{R} population and 54 units from the *rd*^{1} *Opn1mw*^{R} population. The mean±SEM PSTH at each
327 contrast for the *Opn1mw*^{R} (green trace) and *rd*^{1} *Opn1mw*^{R} (black trace) are shown in Figure 3A.
328 Plotting the average change in firing rate over the first 500ms after light onset at each cone contrast
329 demonstrated that the *rd*^{1} *Opn1mw*^{R} mice had a significantly reduced change in firing rate across
330 this contrast range compared to *Opn1mw*^{R} mice and is best fit by two individual curves (Figure 3B; p
331 < 0.0001; F = 44.41). Normalising these changes in firing rate to the maximum response amplitude in
332 each genotype demonstrated that these cells retain contrast sensitivity similar to that of visually
333 intact controls, as both populations are best fit by the same dose-response curve (Figure 3C; R^2 =
334 0.94; p = 0.34, F-test). We confirmed this by plotting the normalised dose-response function for
335 individual units in visually intact and degenerate mice which showed there to be no significant
336 difference in the cone contrast at half maximum response between Opn1mw^{r} mice (Mean±SEM =

337 15.39 ± 1.21) and rd^{1} Opn1mw^{r} mice (Mean±SEM = 15.41 ± 0.97; unpaired t-test; p = 0.988; Figure
338 3D).

339 We continued to ask whether the spatial resolution of cone-driven dLGN responses were impacted
340 by retinal degeneration by mapping receptive fields (RFs) using a vertical bar minimally visible to
341 melanopsin but with ~50% cone contrast in for *Opn1mw^{R}* mice (Figure 4A) and ~70% cone contrast
342 for *rd^{1} Opn1mw^{R}* mice (Figure 4B). We identified 38 single units from *Opn1mw^{R}* mice and 48 single
343 units from *rd^{1} Opn1mw^{R}* mice responsive to this stimulus. The response of two representative units
344 is shown in Figure 4C. For all single units we defined RF by a best fit Gaussian to the relationship
345 between bar position and response amplitude (Figure 4D; R^2 > 0.7; mean = 0.87 for both *rd^{1}*
346 *Opn1mw^{R}* and *Opn1mw^{R}* mice). RF diameter was significantly smaller in *rd^{1} Opn1mw^{R}* mice than
347 *Opn1mw^{R}* mice (Figure 4E; mean±SEM = 9.96°±0.3 and 12.17°±0.5, respectively; p = 0.0005 Unpaired
348 T-test). Similar to the dark-adapted condition, we found the amplitude of these responses to be
349 significantly reduced in *rd^{1} Opn1mw^{R}* mice (7.02 ± 0.8 Spikes/s) compared to *Opn1mw^{R}* mice (10.1 ±
350 1.2 Spikes/s; unpaired T-test = 0.03), even when using stimuli with a higher effective cone contrast in
351 the degenerate mice (Figure 4F). *rd^{1} Opn1mw^{R}* mice also demonstrated a significantly slower time to
352 peak response (177.9ms ± 5.4) compared to *Opn1mw^{R}* mice (112.3ms ± 4.46; unpaired T-test: p
353 <0.0001) for cells which we could record a spatial receptive field (Figure 4G).

354 We finally turned our attention to whether light responses were driven disproportionately by
355 melanopsin at this stage of retinal degeneration. We used the silent substitution approach to
356 present longer (10s full field) steps using our "all photoreceptor" stimulus (which is known to
357 activate melanopsin in the adult wildtype retina (Allen, Storchi et al. 2017)), compared to our "mel-
358 less" stimulus which has an equivalent contrast for cones but minimal contrast for melanopsin. We
359 found 11 units with a sustained OFF phenotype in the *Opn1mw^{R}* population but none in the *rd^{1}*
360 *Opn1mw^{R}* population and as such these units were excluded from any further analysis. Of units

361 excited by the stimuli, 16/76 in *Opn1mw*^{R}, and 14/68 in *rd*^{1} *Opn1mw*^{R} population showed a
362 'sustained' response with maintained firing throughout the light step (Figure 5 A&B), and the
363 remaining 'transient' units excited only at the start and/or end of the light step (Figures 5 D&E).
364 Overall, the response profiles of each population to 'all photoreceptor' and 'mel-less' stimuli were
365 comparable (Figure 5 A&B and D&E). Based upon published work (Brown, Tsujimura et al. 2012,
366 Allen, Storchi et al. 2017) we expect any melanopsin contribution to be apparent in the maintained
367 response of sustained units. Although we found there to be a trend for the magnitude of the "all
368 photoreceptor" sustained response to be larger than the "mel-less" response in both genotypes, we
369 found no significant difference in the total number of spikes throughout the sustained component of
370 the light step (2-10s) of the sustained population in the "all photoreceptor" and "mel-less"
371 conditions in either the *Opn1mw*^{R} mice (Figure 5A; mean±SEM Total Spikes = 18.30 ± 3.0 Spikes and
372 13.67 ± 3.10 Spikes, respectively; p = 0.50; 2-way ANOVA with post hoc Bonferroni correction) or *rd*^{1}
373 *Opn1mw*^{R} mice (Figure 5B; Total Spikes = 17.58 ± 3.25 Spikes and 10.05 ± 2.08 Spikes respectively; p
374 = 0.17; 2-way ANOVA with post hoc Bonferroni correction). As expected, the transient population in
375 showed no significant difference in their response between the "all photoreceptor" and "mel-less"
376 condition over the same duration (Figure 5D; mean±SEM Total Spikes = 1.19 ± 0.59 Spikes and 0.47 ±
377 0.59 Spikes, respectively; p = 0.84; 2-way ANOVA with post hoc Bonferroni correction) or *rd*^{1}
378 *Opn1mw*^{R} mice (Figure 5E; Total Spikes = 3.89 ± 0.78 Spikes and 3.28 ± 0.71 Spikes respectively; p
379 >0.99; 2-way ANOVA with post hoc Bonferroni correction). The lack of a detectable melanopsin
380 contribution to the sustained population in either genotype was surprising in view of previous
381 description of melanopsin signals in the adult wildtype dLGN (Brown, Tsujimura et al. 2012, Davis,
382 Eleftheriou et al. 2015, Allen, Storchi et al. 2017) and could be an effect of this particular
383 developmental stage or simply a limitation in the statistical power of these experiments. In either
384 event, these findings confirm that melanopsin does not make a disproportionate contribution to
385 dLGN light responses at this stage of degeneration in *rd*^{1} mice.

386 **Discussion**

387 To date, much of our understanding of the progress of retinal degeneration has come from
388 anatomical studies (Carterdawson, Lavail et al. 1978, Strettoi, Porciatti et al. 2002, Jones and Marc
389 2005), and more recent electrophysiological recordings (Stasheff 2008, Stasheff, Shankar et al. 2011,
390 Gibson, Fletcher et al. 2013) from the degenerate retina. Few studies have investigated what quality
391 of information these residual light responses support in downstream visual centres in the brain
392 (Drager and Hubel 1978, Chen, Wang et al. 2016) and none have recorded from the dLGN, the major
393 retinorecipient of visual information in mammals (Grubb and Thompson 2003, Huberman and Niell
394 2011). Addressing this deficit is important for understand disease progression and how central vision
395 changes as a function of retinal degeneration. Characterising the residual light responses in this
396 nucleus also provides a context for attempts to restore vision by re-photosensitising the retina (Bi,
397 Cui et al. 2006, Lagali, Balya et al. 2008, Cehajic-Kapetanovic, Eleftheriou et al. 2015, De Silva,
398 Barnard et al. 2017, Mandai, Fujii et al. 2017, McLelland, Lin et al. 2018, Tochitsky, Kienzler et al.
399 2018). If central remodelling processes substantially degrades the visual response in the dLGN, this
400 might provide an additional barrier to success in these approaches. Alternatively, if response
401 properties are largely intact, that would suggest that the early visual system, at least up until the
402 level of the dLGN, remains capable of taking advantage of such interventions to restore not only
403 sensitivity to light, but also the ability to resolve spatial patterns at realistic levels of contrast. The
404 retention of spatial receptive fields in the rd^1 retina in this study is especially encouraging, as it
405 indicates that remodelling has not fundamentally degraded the early visual system's potential for
406 spatial acuity. An important question for future work will be whether receptive fields are similarly
407 retained at later stages in degeneration at which there has been more scope for remodelling. That
408 would inform whether therapeutic interventions should be applied early in degeneration in the hope
409 that they can co-opt and maintain functional circuits or can still be applied in late degeneration.

410 In many aspects we found our electrophysiological recordings in the dLGN were consistent with
411 previous reports of visual responses in the degenerate retina. Light-responses could be readily
412 elicited up to approximately four weeks of age in the *rd*[1] dLGN; however there was a rapid decline in
413 the frequency of encountering light-responsive cells between P18 and P33, consistent with previous
414 anatomical (Carterdawson, Lavail et al. 1978, Jimenez, GarciaFernandez et al. 1996, LaVail, Matthes
415 et al. 1997, Lin, Masland et al. 2009) and electrophysiological (Drager and Hubel 1978, Stasheff 2008,
416 Gibson, Fletcher et al. 2013) descriptions of the progression of cone photoreceptor death in this
417 animal. The variety of the identified light responses in the *rd*[1] dLGN (Transient ON, Transient ON-
418 OFF, Sustained-ON) were also qualitatively similar to those previously described in the juvenile
419 degenerate retina (Stasheff 2008), although we did find a proportional shift towards responses being
420 more transient in the *rd*[1] dLGN. This indicates that visual information can cross the retino-geniculate
421 synapse at these early stages of degeneration. To interrogate this circuitry in more detail, we
422 recorded spatial receptive fields from dLGN neurones and found these to have a mean diameter of
423 9.96° ± 0.3° which is at least as small as in our parallel recordings from age-matched visually intact
424 mice and in agreement with previous recordings from the tectum of young rd[1] mice (11.5°) (Drager
425 and Hubel 1978). It is also within the range previously reported in the dLGN of visually intact adult
426 mice (2-10°) (Grubb and Thompson 2003). One caveat to the interpretation of this data is that we
427 only use vertical bars to map spatial receptive fields in the dLGN. As some dLGN neurones in the
428 mouse exhibit orientation selectivity (Piscopo, El-Danaf et al. 2013, Scholl, Tan et al. 2013, Zhao,
429 Chen et al. 2013), our recordings may in fact underestimate the total number of units for which we
430 could record a spatial receptive field. Nonetheless, our ability to record significant responses to
431 complex spatial stimuli under light-adapted conditions in the *rd*[1] dLGN indicates that, not only is the
432 retinal circuitry linking remaining cones, horizontal cells and bipolar cells at least superficially intact
433 for those dLGN neurones for which we could record spatial receptive fields, but that there is no
434 detectable gross change in the number of retinal ganglion cells converging to an individual dLGN
435 neurone at these early stages of degeneration.

436 While many fundamental aspects of thalamic vision were thus substantially intact at early stages of
437 degeneration there was, of course, a marked effect of retinal degeneration. The most notable
438 impact was on response amplitude and latency. We found that the magnitude (change in firing) of
439 responses to simple light pulses from darkness and contrast steps were significantly reduced in *rd*[1]
440 mice, while latency was significantly increased. These observations are in agreement with previous
441 ERG recordings demonstrating that both a-waves and b-waves of *rd*[1] mice are significantly reduced
442 and delayed as early as at P14 (Strettoi, Porciatti et al. 2002, Gibson, Fletcher et al. 2013) and multi-
443 electrode array recordings from P15 *rd*[1] retinas (Stasheff 2008). They likely reflect not only the loss
444 of the rod population, but also the poor state of surviving cones, which progressively lose their outer
445 segments (LaVail, Matthes et al. 1997, Jones, Watt et al. 2003, Lin, Masland et al. 2009) and have the
446 opsin protein redistributed to be expressed in the plasma membrane of the inner segment (Nir,
447 Agarwal et al. 1989), indicating a loss of efficient photo-transduction. Importantly, the changes in
448 response amplitude we observe under light-adapted conditions did not significantly alter contrast
449 sensitivity (which was similar in the intact and *rd*[1] dLGN) indicating that it need not have a simple
450 consequence for vision under natural light-adapted conditions.

451 A second substantial abnormality of the dLGN light response in *rd*[1] mice was that we failed to
452 identify a single sustained-OFF response. The origin of this deficit is unclear. Whilst anatomical
453 remodelling occurs much later in disease progression (Marc, Jones et al. 2003), neurochemical
454 remodelling, most notably of glutamatergic receptors, has been reported in a number of degenerate
455 strains during the early stages of retinal degeneration (Chua, Fletcher et al. 2009, Puthussery, Gayet-
456 Primo et al. 2009). These include the down regulation of both metabotropic and ionotropic
457 glutamate receptors (Strettoi, Porciatti et al. 2002, Marc, Jones et al. 2007) and the aberrant
458 expression of ionotropic glutamate receptors on ON Cone bipolar cells (Chua, Fletcher et al. 2009).
459 The cone OFF pathway employs ionotropic glutamate receptors on the dendrites of OFF cone bipolar
460 cells (Thoreson and Witkovsky 1999). However, the sustained component of the OFF responses

461 derive from cross over inhibition with ON cone bipolar cells via GABA-ergic Amacrine cells (Rosa,
462 Ruehle et al. 2016). These GABA-ergic Amacrine cells also exhibit abnormal receptor expression at
463 early stages of degeneration (Chua, Fletcher et al. 2009, Srivastava, Sinha-Mahapatra et al. 2015)
464 and as such could result in the creation of corrupted circuitry that fails to faithfully transmit this
465 visual response. Furthermore, it is possible that the segregation of ON and OFF retinogeniculate
466 synapses never fully matures in *rd*^{1} mice. In visually intact animals, the correlated spike timing of pre
467 and post-synaptic neurones is crucial to this segregation and happens within a narrow time window
468 during development (Wong and Oakley 1996, Myhr, Lukasiewicz et al. 2001, Lee, Eglen et al. 2002).
469 However, in *rd*^{1} mice, retinal waves show significant abnormalities in their mean firing rate and
470 inter-burst interval before photoreceptor death in addition to exhibiting sustained hyperactivity and
471 rhythmic oscillations in their firing rate (Stasheff 2008) which could affect the normal refinement of
472 ON-OFF segregation in the dLGN.

473 Although spatial receptive fields were substantially intact in the *rd*^{1} dLGN, our side-by-side
474 comparison with age-matched visually intact *Opn1mw*^{R} mice reveals them to be significantly reduced
475 in diameter (by approximately 3°). One simple potential origin for this effect is the reduced response
476 amplitude, which would make it harder to detect relatively small responses to stimuli located on
477 receptive field margins. This may explain our findings, but we found no correlation between
478 response-amplitude and receptive field diameter between degenerate or visually intact mice (data
479 not shown). A second possibility is that although the retinal mosaic of horizontal cells develops
480 normally in degenerate mice, their synaptic connections with photoreceptors never completely
481 mature (Rossi et al., 2003), and therefore modestly alter the spatial receptive field structure of
482 individual retinal ganglion cells.

483 The final impact of degeneration on dLGN responses that we observed was in the temporal
484 distribution of spike firing. Irradiance steps induce narrow band oscillations in the dLGN of visually

485 intact mice (Storchi, Bedford et al. 2017). We found similar light-induced narrow band oscillations at
486 a frequency of approximately 30Hz in visually intact juvenile mice, but no discernible peaks in the
487 power spectrum across a wide range of frequencies (0-50Hz) in the degenerate dLGN. Oscillations in
488 the dLGN, and those recorded from the visual cortex in visually intact mice (Saleem, Lien et al. 2017),
489 are believed to be at least in part inherited from network interactions in the retina (Storchi, Bedford
490 et al. 2017) and play a role in improving the signal:noise ratio of neighbouring neurones in the dLGN
491 network. Thus, the lack of any narrowband oscillations in the degenerate dLGN suggests the
492 impairment of some retinal networks at these early stages which may have significant implications
493 for visual processing (Koepsell, Wang et al. 2009), and is supported by the loss of ERG signals by P14
494 in *rd*^{1} mice (Strettoi, Porciatti et al. 2002) and the appearance of correlated firing and spontaneous
495 hyperactivity recorded in retinal ganglion cells in these mice (Menzler and Zeck 2011, Stasheff,
496 Shankar et al. 2011, Goo, Park et al. 2016).

497 As the prospect of restoring photosensitivity to the degenerate retina increasingly becomes a reality,
498 it is important to turn attention to the central response to these new signals as abnormalities in the
499 functioning of downstream visual circuits may impose a significant constraint on the quality of
500 restored vision. Our data overall support an optimistic view of this problem for potential therapies.
501 Thus, while aspects of the dLGN light response are certainly abnormal in the juvenile *rd*^{1} mice, they
502 are not obviously more disrupted than has been reported in the retina and key features, especially
503 contrast sensitivity and receptive field size, are retained. This implies that at least at the level of the
504 dLGN, central reorganisation or secondary degeneration need not pose a barrier to the efficacy of
505 restored photoreception. An important caveat to this conclusion, however, is that the *rd*^{1} mouse has
506 very rapid retinal degeneration which begins during visual system development it therefore may not
507 be the most suitable model to study more gradual changes in circuitry that could occur in humans
508 who would typically experience progressive degeneration over many years.

509 **References**

510 Allen, A. E., R. Storchi, F. P. Martial, R. A. Bedford and R. J. Lucas (2017). "Melanopsin Contributions
511 to the Representation of Images in the Early Visual System." Current Biology **27**(11): 1623-+.
512 Bi, A. D., J. J. Cui, Y. P. Ma, E. Olshevskaya, M. L. Pu, A. M. Dizhoor and Z. H. Pan (2006). "Ectopic
513 expression of a microbial-type rhodopsin restores visual responses in mice with photoreceptor
514 degeneration." Neuron **50**(1): 23-33.
515 Brown, T. M., C. Gias, M. Hatori, S. R. Keding, M. a. Semo, P. J. Coffey, J. Gigg, H. D. Piggins, S. Panda
516 and R. J. Lucas (2010). "Melanopsin Contributions to Irradiance Coding in the Thalamo-Cortical Visual
517 System." Plos Biology **8**(12).
518 Brown, T. M., S. Tsujimura, A. E. Allen, J. Wynne, R. Bedford, G. Vickery, A. Vugler and R. J. Lucas
519 (2012). "Melanopsin-Based Brightness Discrimination in Mice and Humans." Current Biology **22**(12):
520 1134-1141.
521 Carterdawson, L. D. and M. M. Lavail (1979). "RODS AND CONES IN THE MOUSE RETINA .1.
522 STRUCTURAL-ANALYSIS USING LIGHT AND ELECTRON-MICROSCOPY." Journal of Comparative
523 Neurology **188**(2): 245-262.
524 Carterdawson, L. D., M. M. Lavail and R. L. Sidman (1978). "DIFFERENTIAL EFFECT OF RD MUTATION
525 ON RODS AND CONES IN MOUSE RETINA." Investigative Ophthalmology & Visual Science **17**(6): 489-
526 498.
527 Cehajic-Kapetanovic, J., C. Eleftheriou, A. E. Allen, N. Milosavljevic, A. Pienaar, R. Bedford, K. E. Davis,
528 P. N. Bishop and R. J. Lucas (2015). "Restoration of Vision with Ectopic Expression of Human Rod
529 Opsin." Current Biology **25**(16): 2111-2122.
530 Chen, K., Y. Wang, X. H. Liang, Y. H. Zhang, T. K. Ng and L. L. H. Chan (2016). "Electrophysiology
531 Alterations in Primary Visual Cortex Neurons of Retinal Degeneration (S334ter-line-3) Rats."
532 Scientific Reports **6**.
533 Choi, H., L. Zhang, M. S. Cembrowski, C. F. Sabottke, A. L. Markowitz, D. A. Butts, W. L. Kath, J. H.
534 Singer and H. Riecke (2014). "Intrinsic bursting of AII amacrine cells underlies oscillations in the rd1
535 mouse retina." Journal of Neurophysiology **112**(6): 1491-1504.
536 Chua, J., E. L. Fletcher and M. Kalloniatis (2009). "Functional Remodeling of Glutamate Receptors by
537 Inner Retinal Neurons Occurs From an Early Stage of Retinal Degeneration." Journal of Comparative
538 Neurology **514**(5): 473-491.
539 Davis, K. E., C. G. Eleftheriou, A. E. Allen, C. A. Procyk and R. J. Lucas (2015). "Melanopsin-Derived
540 Visual Responses under Light Adapted Conditions in the Mouse dLGN." Plos One **10**(3).
541 De Silva, S. R., A. R. Barnard, S. Hughes, S. K. E. Tam, C. Martin, M. S. Singh, A. O. Barnea-Cramer, M.
542 E. McClements, M. J. During, S. N. Peirson, M. W. Hankins and R. E. MacLaren (2017). "Long-term
543 restoration of visual function in end-stage retinal degeneration using subretinal human melanopsin
544 gene therapy." Proceedings of the National Academy of Sciences of the United States of America
545 **114**(42): 11211-11216.
546 Drager, U. C. and D. H. Hubel (1978). "STUDIES OF VISUAL FUNCTION AND ITS DECAY IN MICE WITH
547 HEREDITARY RETINAL DEGENERATION." Journal of Comparative Neurology **180**(1): 85-114.
548 Gibson, R., E. L. Fletcher, A. J. Vingrys, Y. Zhu, K. A. Vessey and M. Kalloniatis (2013). "Functional and
549 neurochemical development in the normal and degenerating mouse retina." Journal of Comparative
550 Neurology **521**(6): 1251-1267.

551 Goo, Y. S., D. J. Park, J. R. Ahn and S. S. Senok (2016). "Spontaneous Oscillatory Rhythms in the
552 Degenerating Mouse Retina Modulate Retinal Ganglion Cell Responses to Electrical Stimulation."
553 Frontiers in Cellular Neuroscience **9**.
554 Govardovskii, V. I., N. Fyhrquist, T. Reuter, D. G. Kuzmin and K. Donner (2000). "In search of the
555 visual pigment template." Visual Neuroscience **17**(4): 509-528.
556 Greferath, U., H. C. Goh, P. Y. Chua, E. Astrand, E. E. O'Brien, E. L. Fletcher and M. Murphy (2009).
557 "Mapping Retinal Degeneration and Loss-of-Function in Rd-FTL Mice." Investigative Ophthalmology
558 & Visual Science **50**(12): 5955-5964.
559 Grubb, M. S. and I. D. Thompson (2003). "Quantitative characterization of visual response properties
560 in the mouse dorsal lateral geniculate nucleus." Journal of Neurophysiology **90**(6).
561 Huberman, A. D. and C. M. Niell (2011). "What can mice tell us about how vision works?" Trends in
562 Neurosciences **34**(9): 464-473.
563 Jimenez, A. J., J. M. GarciaFernandez, B. Gonzalez and R. G. Foster (1996). "The spatio-temporal
564 pattern of photoreceptor degeneration in the aged rd/rd mouse retina." Cell and Tissue Research
565 **284**(2): 193-202.
566 Jones, B. W. and R. E. Marc (2005). "Retinal remodeling during retinal degeneration." Experimental
567 Eye Research **81**(2): 123-137.
568 Jones, B. W., C. B. Watt, J. M. Frederick, W. Baehr, C. K. Chen, E. M. Levine, A. H. Milam, M. M. Lavail
569 and R. E. Marc (2003). "Retinal remodeling triggered by photoreceptor degenerations." Journal of
570 Comparative Neurology **464**(1): 1-16.
571 Koepsell, K., X. Wang, V. Vaingankar, Y. Wei, Q. Wang, D. L. Rathbun, W. M. Usrey, J. A. Hirsch and F.
572 T. Sommer (2009). "Retinal oscillations carry visual information to cortex." Frontiers in systems
573 neuroscience **3**: 4-4.
574 Lagali, P. S., D. Balya, G. B. Awatramani, T. A. Munch, D. S. Kim, V. Busskamp, C. L. Cepko and B.
575 Roska (2008). "Light-activated channels targeted to ON bipolar cells restore visual function in retinal
576 degeneration." Nature Neuroscience **11**(6): 667-675.
577 LaVail, M. M., M. T. Matthes, D. Yasumura and R. H. Steinberg (1997). "Variability in rate of cone
578 degeneration in the retinal degeneration (rd/rd) mouse." Experimental Eye Research **65**(1): 45-50.
579 Lee, C. W., S. J. Eglen and R. O. L. Wong (2002). "Segregation of ON and OFF retinogeniculate
580 connectivity directed by patterned spontaneous activity." Journal of Neurophysiology **88**(5): 2311-
581 2321.
582 Lin, B., R. H. Masland and E. Strettoi (2009). "Remodeling of cone photoreceptor cells after rod
583 degeneration in rd mice." Experimental Eye Research **88**(3): 589-599.
584 Lin, B. and E. B. Peng (2013). "Retinal Ganglion Cells are Resistant to Photoreceptor Loss in Retinal
585 Degeneration." Plos One **8**(6).
586 Mandai, M., M. Fujii, T. Hashiguchi, G. A. Sunagawa, S. Ito, J. A. Sun, J. Kaneko, J. Sho, C. Yamada and
587 M. Takahashi (2017). "iPSC-Derived Retina Transplants Improve Vision in rdl End-Stage Retinal-
588 Degeneration Mice." Stem Cell Reports **8**(1): 69-83.
589 Marc, R. E., B. W. Jones, J. R. Anderson, K. Kinard, D. W. Marshak, J. H. Wilson, T. Wensel and R. J.
590 Lucas (2007). "Neural reprogramming in retinal degeneration." Investigative Ophthalmology & Visual
591 Science **48**(7): 3364-3371.
592 Marc, R. E., B. W. Jones, C. B. Watt and E. Strettoi (2003). "Neural remodeling in retinal
593 degeneration." Progress in Retinal and Eye Research **22**(5): 607-655.
594 McLelland, B. T., B. Lin, A. Mathur, R. B. Aramant, B. B. Thomas, G. Nistor, H. S. Keirstead and M. J.
595 Seiler (2018). "Transplanted hESC-Derived Retina Organoid Sheets Differentiate, Integrate, and

596 Improve Visual Function in Retinal Degenerate Rats." Investigative Ophthalmology & Visual Science
597 **59**(6): 2586-2603.
598 Menzler, J. and G. Zeck (2011). "Network Oscillations in Rod-Degenerated Mouse Retinas." Journal of
599 Neuroscience **31**(6): 2280-2291.
600 Myhr, K. L., P. D. Lukasiewicz and R. O. L. Wong (2001). "Mechanisms underlying developmental
601 changes in the firing patterns of ON and OFF retinal ganglion cells during refinement of their central
602 projections." Journal of Neuroscience **21**(21): 8664-8671.
603 Nir, I., N. Agarwal, G. Sagie and D. S. Papermaster (1989). "OPSIN DISTRIBUTION AND SYNTHESIS IN
604 DEGENERATING PHOTORECEPTORS OF RD MUTANT MICE." Experimental Eye Research **49**(3): 403-
605 421.
606 Ogilvie, J. M., T. Tenkova, J. M. Lett, J. Speck, M. Landgraf and M. S. Silverman (1997). "Age-related
607 distribution of cones and ON-bipolar cells in the rd mouse retina." Current Eye Research **16**(3): 244-
608 251.
609 Peirce, J. W. (2008). "Generating Stimuli for Neuroscience Using PsychoPy." Frontiers in
610 neuroinformatics **2**: 10-10.
611 Piscopo, D. M., R. N. El-Danaf, A. D. Huberman and C. M. Niell (2013). "Diverse Visual Features
612 Encoded in Mouse Lateral Geniculate Nucleus." Journal of Neuroscience **33**(11): 4642-4656.
613 Procyk, C. A., C. G. Eleftheriou, R. Storchi, A. E. Allen, N. Milosavljevic, T. M. Brown and R. J. Lucas
614 (2015). "Spatial receptive fields in the retina and dorsal lateral geniculate nucleus of mice lacking
615 rods and cones." Journal of Neurophysiology **114**(2): 1321-1330.
616 Puthussery, T., J. Gayet-Primo, S. Pandey, R. M. Duvoisin and W. R. Taylor (2009). "Differential loss
617 and preservation of glutamate receptor function in bipolar cells in the rd10 mouse model of retinitis
618 pigmentosa." European Journal of Neuroscience **29**(8): 1533-1542.
619 Rosa, J. M., S. Ruehle, H. Y. Ding and L. Lagnado (2016). "Crossover Inhibition Generates Sustained
620 Visual Responses in the Inner Retina." Neuron **90**(2): 308-319.
621 Saleem, A. B., A. D. Lien, M. Krumin, B. Haider, M. R. Roson, A. Ayaz, K. Reinhold, L. Busse, M.
622 Carandini and K. D. Harris (2017). "Subcortical Source and Modulation of the Narrowband Gamma
623 Oscillation in Mouse Visual Cortex." Neuron **93**(2): 315-322.
624 Scholl, B., A. Y. Y. Tan, J. Corey and N. J. Priebe (2013). "Emergence of Orientation Selectivity in the
625 Mammalian Visual Pathway." Journal of Neuroscience **33**(26): 10616-+.
626 Smallwood, P. M., B. P. Olveczky, G. L. Williams, G. H. Jacobs, B. E. Reese, M. Meister and J. Nathans
627 (2003). "Genetically engineered mice with an additional class of cone photoreceptors: Implications
628 for the evolution of color vision." Proceedings of the National Academy of Sciences of the United
629 States of America **100**(20): 11706-11711.
630 Srivastava, P., S. K. Sinha-Mahapatra, A. Ghosh, I. Srivastava and N. K. Dhingra (2015). "Differential
631 Alterations in the Expression of Neurotransmitter Receptors in Inner Retina following Loss of
632 Photoreceptors in rd1 Mouse." Plos One **10**(4).
633 Stasheff, S. F. (2008). "Emergence of sustained spontaneous hyperactivity and temporary
634 preservation of OFF responses in ganglion cells of the retinal degeneration (rd1) mouse." Journal of
635 Neurophysiology **99**(3): 1408-1421.
636 Stasheff, S. F., M. Shankar and M. P. Andrews (2011). "Developmental time course distinguishes
637 changes in spontaneous and light-evoked retinal ganglion cell activity in rd1 and rd10 mice." Journal
638 of Neurophysiology **105**(6): 3002-3009.

Storchi, R., R. A. Bedford, F. P. Martial, A. E. Allen, J. Wynne, M. A. Montemurro, R. S. Petersen and R. J. Lucas (2017). "Modulation of Fast Narrowband Oscillations in the Mouse Retina and dLGN According to Background Light Intensity." Neuron **93**(2): 299-307.

Strettoi, E. and V. Pignatelli (2000). "Modifications of retinal neurons in a mouse model of retinitis pigmentosa." Proceedings of the National Academy of Sciences of the United States of America **97**(20): 11020-11025.

Strettoi, E., V. Pignatelli, C. Rossi, V. Porciatti and B. Falsini (2003). "Remodeling of second-order neurons in the retina of rd/rd mutant mice." Vision Research **43**(8): 867-877.

Strettoi, E., V. Porciatti, B. Falsini, V. Pignatelli and C. Rossi (2002). "Morphological and functional abnormalities in the inner retina of the rd/rd mouse." Journal of Neuroscience **22**(13): 5492-5504.

Thoreson, W. B. and P. Witkovsky (1999). "Glutamate receptors and circuits in the vertebrate retina." Progress in Retinal and Eye Research **18**(6).

Tochitsky, I., M. A. Kienzler, E. Isacoff and R. H. Kramer (2018). "Restoring Vision to the Blind with Chemical Photoswitches." Chemical Reviews **118**(21): 10748-10773.

Vugler, A. A., M. Semo, A. Joseph and G. Jeffery (2008). "Survival and remodeling of melanopsin cells during retinal dystrophy." Visual Neuroscience **25**(2).

Wong, R. O. L. and D. M. Oakley (1996). "Changing patterns of spontaneous bursting activity of on and off retinal ganglion cells during development." Neuron **16**(6): 1087-1095.

Zhao, X. Y., H. Chen, X. R. Liu and J. H. Cang (2013). "Orientation-selective Responses in the Mouse Lateral Geniculate Nucleus." Journal of Neuroscience **33**(31): 12751-+.

Additional Information

Competing interests

No conflicts of interest, financial or otherwise, are declared by the authors.

Author contributions

CAP, AEA, FPM and RJL, conception and design of work; CAP, AEA and RJL acquisition, analysis and interpretation of the data; CAP, AEA, FPM and RJL, drafting and revising work critically for important intellectual content and CAP, AEA, FPM and RJL approved the final version of the manuscript. All experiments were carried out at the University of Manchester in the laboratory of Professor Robert J Lucas.

Funding

This research was supported by a grant from the European Research Council (268970) awarded to RJL.

Acknowledgements

The authors thank J. Wynne for technical assistance

680 **Figure Legends**

681

682 **Figure 1: Design and validation of silent substitution stimuli. (A) The** *Opn1mw^R* retina expresses four spectrally distinct
683 opsins in the retina: S-cone opsin (λ_{max} = 390; purple), Melanopsin (λ_{max}= 480nm; blue), Rod opsin (λ_{max} = 498nm; black),
684 however the Human the L-cone opsin (λ_{max} = 556nm; green) is knocked into the genome in place of the native mouse green
685 cone opsin (λ_{max} = 508nm). The *rd^1 Opn1mw^R* retina expresses three spectrally distinct and functional photoreceptors in the
686 retina: S-cones, L-Cones and melanopsin. Rod photoreceptors are rendered functionless from birth due to the *rd^1* mutation
687 and rapidly degenerate by Post Natal Day 17. **(B)** The output of four LEDs (peak emissions = 405nm, 455nm, 525nm,
688 630nm) and a laser (peak emission = 561nm) were used to produce three spectra (1 = green trace, 2 = pink trace, and 3 =
689 orange trace). Transition from Spectrum 1 to 3 ("all photoreceptor" stimulus) presented a positive contrast for rod opsin,
690 cone opsins and melanopsin. Transition from Spectrum 2 to 3 ("mel-less") provided the same contrast for rod and cone
691 photoreceptors as the "all photoreceptor" condition but had a minimal melanopsin contrast. (**C; left**) The effective photon
692 flux for each photopigment in the *Opn1mw^R* retina (L-Cone opsin, S-Cone opsin, Rod opsin and melanopsin) when
693 presented with Spectra 1, 2 and 3. (**C**; *right*) Michaelson contrast calculated for L-Cone opsin, S-Cone opsin, rod opsin and
694 melanopsin for transitions in the "all photoreceptor" and "mel-less" conditions. Peristimulus time histograms (PSTH)
695 demonstrating the Mean±SEM light-response of dLGN units from the **(D)** *Opn1mw^R* population and **(E)** *rd^1 Opn1mw^R*
696 population in response to 50 presentations of the "all photoreceptor" (black trace) and "mel-less" (red trace) stimuli. Data
697 shown is baseline subtracted (time bin = 0.01s). **(F)** Peak response amplitude for single dLGN units was not significantly
698 different when comparing the "all photoreceptor" and "mel-less" conditions for *Opn1mw^R* mice (mean±SEM = 26.33 ± 1.52
699 Spikes/s and 24.38 ± 1.73 Spikes/s, respectively; p = 0.09) and *rd^1 Opn1mw^R* mice (mean±SEM = 20.25 ± 1.73 Spikes/s and
700 19.58 ± 1.84 Spikes/s, respectively; p = 0.79). **(G)** Latency to peak response for single dLGN units was also not significantly
701 different when comparing the "all photoreceptor" and "mel-less" conditions for *Opn1mw^R* mice (mean±SEM = 154.26 ±
702 4.87ms and 156.55 ± 4.68ms, respectively; p = 0.97) and *rd^1 Opn1mw^R* mice (mean±SEM = 183.13 ± 5.28ms and 174.93 ±
703 6.63ms, respectively; p = 0.27).

704

705 **Figure 2: Dark-adapted light-responses in the *rd^1 Opn1mw^R* dLGN. (A)** Representative image of DiI labelled electrode tract
706 (blue) superimposed with channels of the A4X8-5 mm-50-200-413 recording electrode (grey circles) in an *rd^1 Opn1mw^R*
707 mouse confirming placement of recording electrode (Paxinos and Watson mouse atlas used to confirm placement of the
708 recording electrode in the dLGN and is outlined by a black dotted line). **(B)** Representative reconstruction of light-
709 responsive channels found in the *rd^1 Opn1mw^R* dLGN recording from *(A)* in response to full field 200ms flashes (2.50×10^{14}
710 photons cm^{-2} s^{-1}) from darkness. **(C)** Plotting the number of light-responsive units per electrode placement as a function of

711 age demonstrated a significant decrease in light-responsive units in the *rd*^{1} *Opn1mw*^{R} population (green crosses; slope = -
712 1.35; p = 0.003) compared to *Opn1mw*^{R} mice (black crosses; slope = 0.67; p = 0.06). **(D)** Single unit light-responses could be
713 categorised as transient or sustained in response to a 10s light-step (irradiance =2.50x10^{14} photons cm^{-2} s^{-1}) from darkness
714 (n = 135 light-responsive units from eight *Opn1mw*^{R} mice & 90 light-responsive units from six *rd*^{1} *Opn1mw*^{R} mice. Transient
715 cells could be further subdivided in transient ON and transient ON-OFF responses to light whilst sustained cells
716 demonstrated a sustained ON or sustained OFF response to light (percentage of cells in each genotype with response type
717 shown top right). **(E)** Peak ON response amplitude was calculated for transient (transient ON, transient ON-OFF) and
718 sustained (sustained ON) units for both *Opn1mw*^{R} *(green data points)* and *rd*^{1} *Opn1mw*^{R} mice (black data points). There was
719 no significant difference between transient and sustained populations for *Opn1mw*^{R} (p = 0.83) and *rd*^{1} *Opn1mw*^{R} units (p =
720 0.15), but there was a significant difference when comparing transient units between *Opn1mw*^{R} and *rd*^{1} *Opn1mw*^{R} (p =
721 0.026) and sustained units in the *Opn1mw*^{R} dLGN and transient units in the *rd*^{1} *Opn1mw*^{R} dLGN (p=0.0002; 2-Way ANOVA
722 with post hoc Bonferroni correction). **(F)** Time to peak response was significantly faster for *Opn1mw*^{R} dLGN units. Transient
723 units in the *Opn1mw*^{R} dLGN were significantly faster than transient (p <0.0001) and sustained units (p = 0.0085) in the *rd*^{1}
724 *Opn1mw*^{R} units. Sustained units in the *Opn1mw*^{R} dLGN were also significantly faster than transient units in the *rd*^{1}
725 *Opn1mw*^{R} dLGN (p = 0.0009) but not significantly faster than sustained units (p = 0.20; 2-Way ANOVA with post hoc
726 Bonferroni correction). **(G)** The integrated PSTH of the sustained component of the light-response was significantly larger in
727 *Opn1mw*^{R} units compared to *rd*^{1} *Opn1mw*^{R} units (mean±SEM Total Spikes = 112.1 ± 14.52 Spikes and 20.36 ± 3.28 Spikes,
728 respectively; p = 0.0028; unpaired T-test). **(H)** Normalised Power Spectrum Density (PSD) of light-responsive units during a
729 10s light pulse demonstrates that a robust peak can be identified in the *Opn1mw*^{R} population (green trace; 31.3±0.39Hz)
730 but no discernible peak in the in the *rd*^{1} *Opn1mw*^{R} population (black trace).
731
732 **Figure 3: Contrast sensitivity in the *rd*^{1} *Opn1mw*^{R} dLGN (A)** Mean ± S.E.M. peristimulus time histograms (PSTH) of light
733 responsive units in the dLGN of *Opn1mw*^{R} (green trace, n = 61 units) and *rd*^{1} *Opn1mw*^{R} (black trace; n= 54 units) in response
734 to 20 repeats of a 1 second light-step at eight increasing cone contrasts (1%, 2%, 5%, 16%, 20%, 30%, 40% and 50%)
735 presented against a background of irradiance = 2.64x10^{14} photons cm^{-2} s^{-1} (time bin = 0.01s; inter stimulus interval = 5
736 seconds; Scale bar = 5 Spikes/s). **(B)** Mean±S.E.M. change in firing rate over the first 500ms of the light-step plotted as a
737 function of cone contrast (mean of contrast for L-cone and S-cone). *Opn1mw*^{R} mice (green trace) showed significantly larger
738 amplitude response than *rd*^{1} *Opn1mw*^{R} mice (black trace) as both populations are best fit by two separate dose-response
739 curves (p < 0.001, F-test = 44.1; *Opn1mw*^{R} R^2 = 0.95; *rd*^{1} *Opn1mw*^{R} R^2 = 0.97). **(C)** Normalising peak response amplitude of
740 the data in ***(B)*** to maximum response for that genotype allowed the data for *Opn1mw*^{R} (green trace) and *rd*^{1} *Opn1mw*^{R}
741 mice (black trace) to be best fit by a single curve (F-test = 0.798; R^2 = 0.94). **(D)** Normalising peak response amplitude of the
742 data and fitting a dose-response curve for individual units (R^2>0.6) showed there was no significant difference in the cone

743 contrast at half maximum response between Opn1mw^{r}mice (green trace; Mean±SEM = 15.39 ± 1.21) and rd^{1} Opn1mw^{r}
744 mice (black trace; Mean±SEM = 15.41 ± 0.97; unpaired t-test; p = 0.988).
745
746 **Figure 4: Spatial receptive fields in the *rd^{1} Opn1mw^{R}* dLGN (A&B)** The effective photon flux of the background and bar
747 stimuli used for receptive field mapping in *(A) Opn1mw^{R}* and *(B) rd^{1} Opn1mw^{R}* mice, with calculated Michaelson contrast,
748 for each photopigment. Note that rod contrast is not relevant for *rd^{1}* mice as these animals lack rods at the age of
749 recording. **(C)** Heat map for representative single units from the dLGN of an *Opn1mw^{R}* (top) and *rd^{1} Opn1mw^{R}* (bottom)
750 mouse showing change in firing rate (spikes/s; scale to right) in response to appearance of vertical bars (250ms starting at
751 time 0; 13° width, at 4.5° resolution) as a function of location on azimuth of bar centre. **(D)** Peak response amplitude
752 (Mean±S.E.M change in firing rate) as a function of bar position for the two units in *(C)* fit with a Gaussian function. **(E)** Box
753 and whisker plot showing that receptive field diameter for all light-responsive units was significantly larger in *Opn1mw^{R}*
754 (Mean±S.E.M = 12.17° ± 0.5; n = 38 units; green bar) compared to *rd^{1} Opn1mw^{R}* mice (9.96° ± 0.3; n = 48 units; black bar;
755 unpaired t-test: p= 0.0005) (box = interquartile range; line in box = median; cross = mean; whiskers = minimum to
756 maximum range). **(F)** Peak response amplitude was significantly larger in *Opn1mw^{R}* (Mean±S.E.M change in firing 10.1 ± 1.2
757 spikes/s) than *rd^{1} Opn1mw^{R}* mice (7.02 ± 0.8 spikes/s; unpaired t-test = 0.03). **(G)** Response latency was significantly
758 increased in *rd^{1} Opn1mw^{R}* (Mean±S.E.M 177.9ms ± 5.4) than *Opn1mw^{R}* mice (112.3ms ± 4.46; unpaired t-test: p <0.0001).
759
760 **Figure 5: Melanopsin signals are absent from the juvenile dLGN.** PSTH (mean±SEM) change in firing rate of single units
761 with a sustained response phenotype from the dLGN of **(A)** *Opn1mw^{R}* (n = 16 single units from 8 mice) and **(B)** *rd^{1}*
762 *Opn1mw^{R}* (n = 14 single units from 6 mice) mice, associated with "all photoreceptor" and "mel-less" conditions (black and
763 red traces respectively *A&B*; stimulus onset at time = 0; duration 10s). **(C)** Total number of Spikes (integrated sum of spikes
764 between 2-10s during the light pulse) for the sustained population of cells showed no significant difference between "all
765 photoreceptor" and "mel-less" conditions for *Opn1mw^{R}* mice (mean±SEM Total Spikes = 18.3 ± 3.0 Spikes and 13.67 ± 3.1
766 Spikes, respectively; p = 0.5; 2-way ANOVA with post hoc Bonferroni correction) or *rd^{1} Opn1mw^{R}* mice (mean±SEM Total
767 Spikes = 17.58 ± 3.25 Spikes and 10.05 ± 2.08 Spikes respectively; p = 0.17; 2-way ANOVA with post hoc Bonferroni
768 correction). Total number of Spikes for 'transient' units in **(D)** *Opn1mw^{R}* mice (n = 60 units) and **(E)** *rd^{1} Opn1mw^{R}* mice (n =
769 50 units) associated with "all photoreceptor" and "mel-less" conditions (black and red traces respectively; stimulus onset at
770 time = 0; duration 10s). **(F)** Total number of Spikes (integrated sum of spikes between 2-10s during the light pulse) for the
771 transient population of cells showed no significant difference between "all photoreceptor" and "mel-less" conditions for
772 *Opn1mw^{R}* mice (mean±SEM Total Spikes = 1.19 ± 0.59 Spikes and 0.47 ± 0.59 Spikes, respectively; p = 0.84; 2-way ANOVA
773 with post hoc Bonferroni correction) or *rd^{1} Opn1mw^{R}* mice (mean±SEM Total Spikes = 3.89 ± 0.78 Spikes and 3.28 ± 0.71

774 Spikes, respectively; $p > 0.99$; 2-way ANOVA with post hoc Bonferroni correction). All graphs show baseline subtracted

775 firing rate in spikes/s (Mean±S.E.M.) in 0.25s time bins.

A

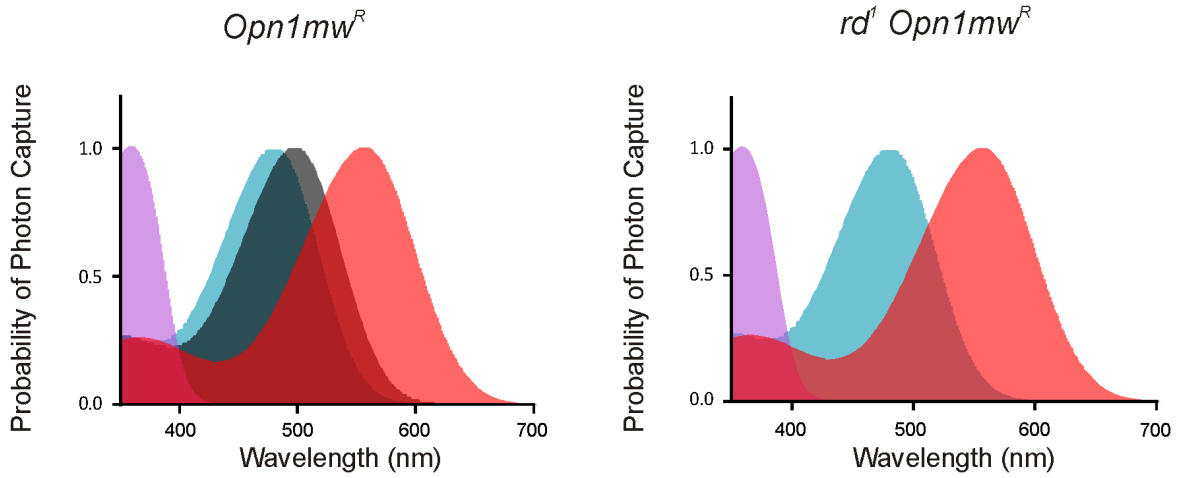

B

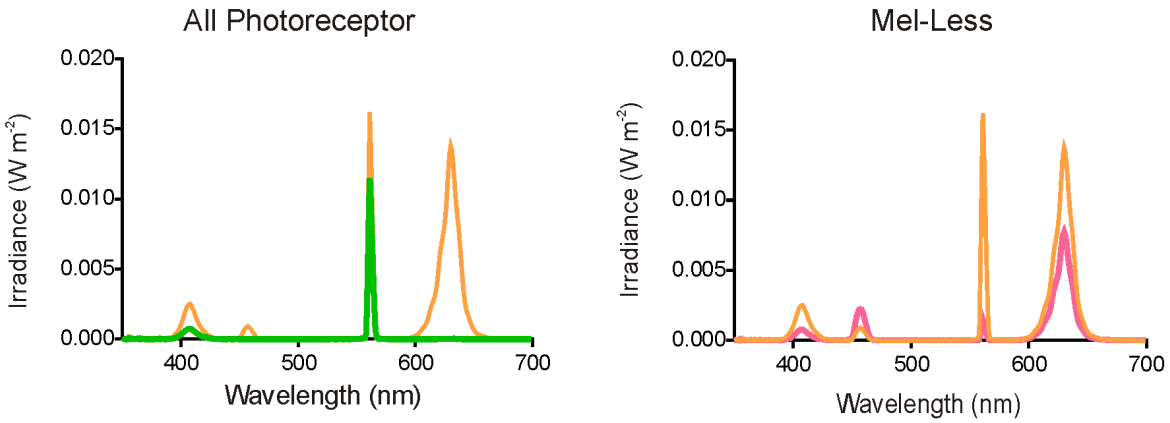

C

	Irradiance (Photons cm^{-2} s^{-1})				
Spectrum	**Total**	**L-Cone**	**S-Cone**	**Rod**	**Mel**
1	1.5E+13	1.3E+13	2.5E+11	3.6E+12	1.6E+12
2	5.0E+13	1.2E+13	2.6E+11	4.0E+12	4.7E+12
3	1.0E+14	3.7E+13	7.9E+11	7.5E+12	5.2E+12

		Photoreceptor Contrast (%)			
Spectra Change	**Stimulus Condition**	**L-Cone**	**S-Cone**	**Rod**	**Mel**
1-3	"All Photoreceptor"	47.0	50.9	34.7	51.9
2-3	"Mel-Less"	49.1	50.2	29.9	5.5

D

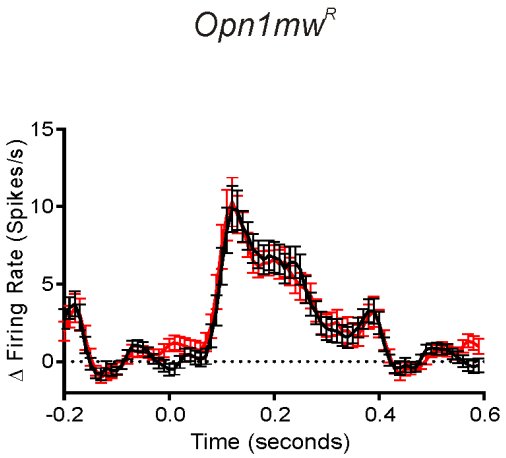

E

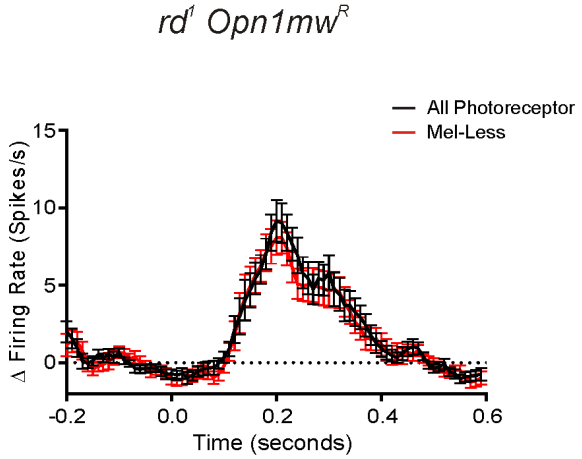

F

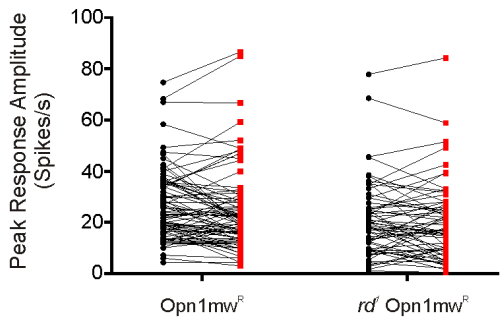

G

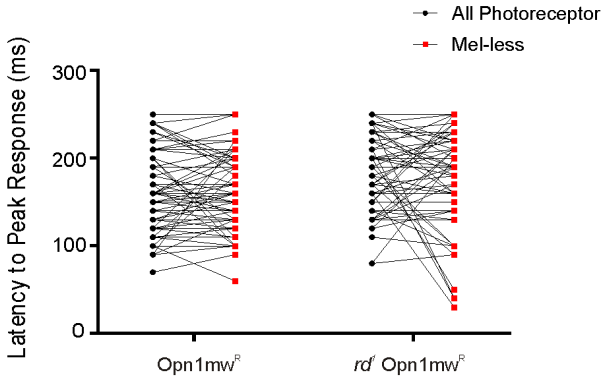

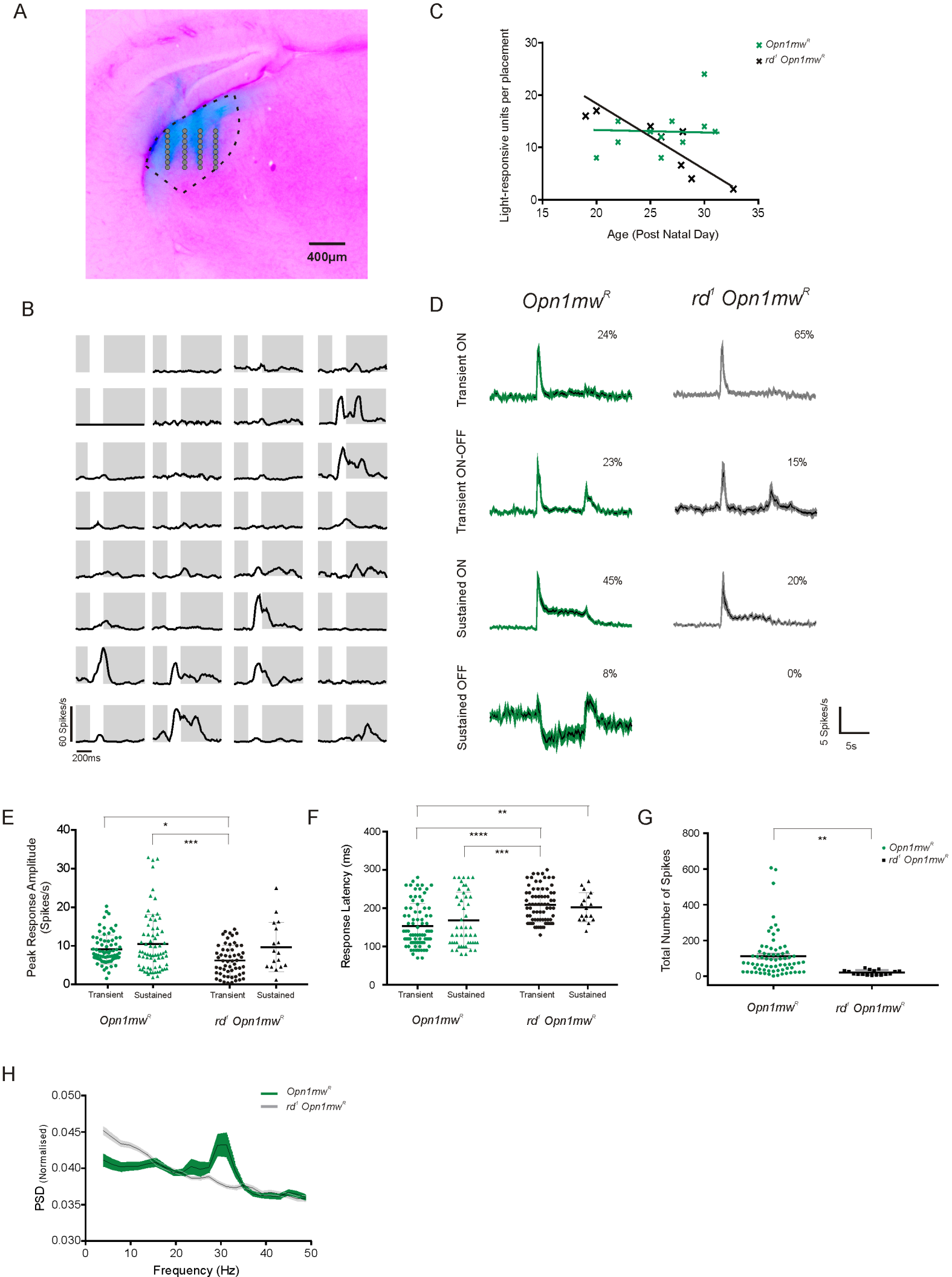
A
400µm
C
Light-responsive units per placement
Age (Post Natal Day)
Opn1mw^R
rd^1 Opn1mw^R
B
60 Spikes/s
200ms
D
Opn1mw^R
rd^1 Opn1mw^R
Transient ON
Transient ON-OFF
Sustained ON
Sustained OFF
24%
65%
23%
15%
45%
20%
8%
0%
5 Spikes/s
5s
E
Peak Response Amplitude (Spikes/s)
Transient
Sustained
Opn1mw^R
rd^1 Opn1mw^R
F
Response Latency (ms)
G
Total Number of Spikes
H
PSD (Normalised)
Frequency (Hz)

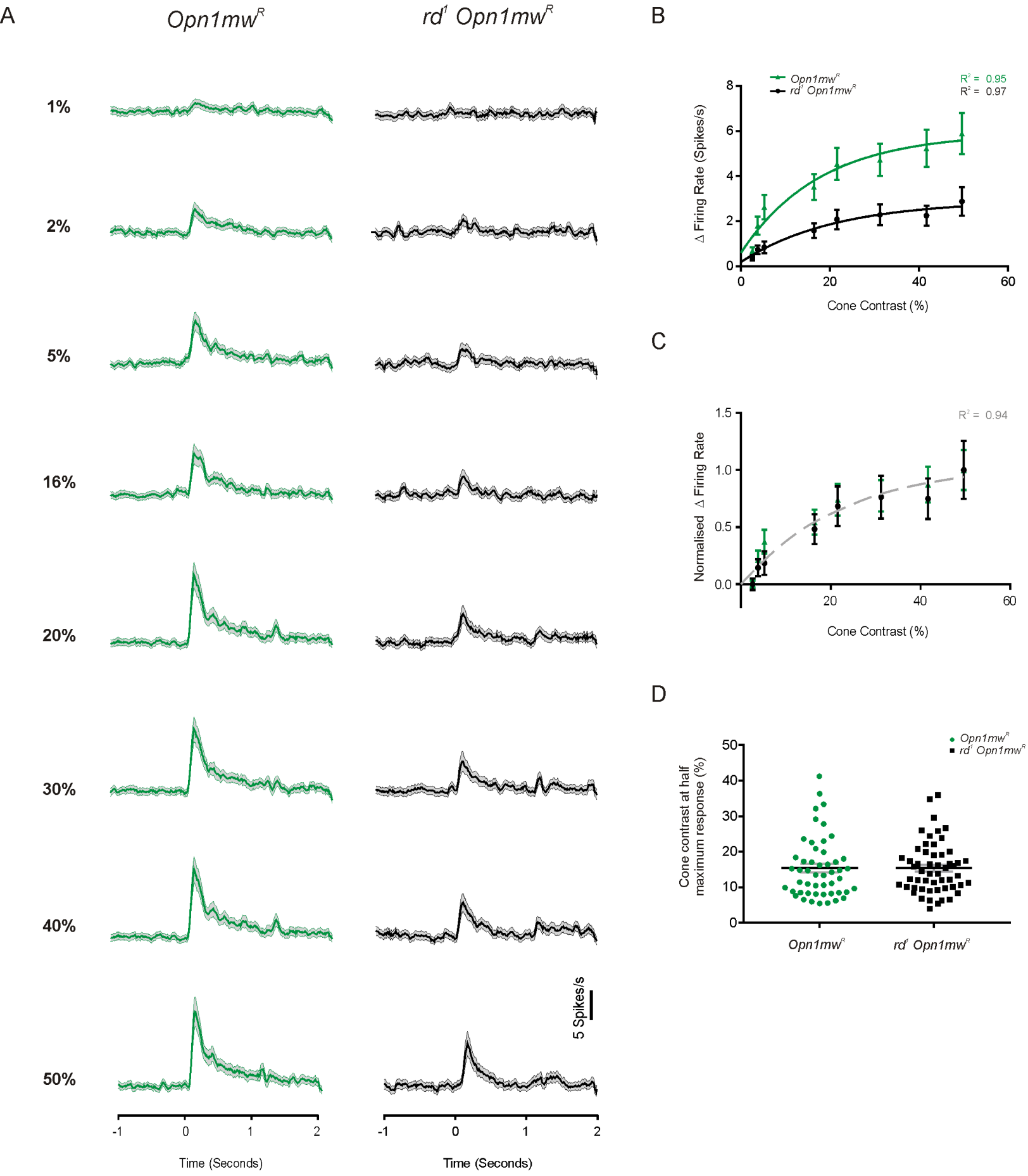
A
Opn1mw^R
rd1 Opn1mw^R
1%
2%
5%
16%
20%
30%
40%
50%
5 Spikes/s
-1
0
1
2
Time (Seconds)
B
Opn1mw^R
rd1 Opn1mw^R
R² = 0.95
R² = 0.97
Δ Firing Rate (Spikes/s)
Cone Contrast (%)
C
R² = 0.94
Normalised Δ Firing Rate
Cone Contrast (%)
D
Cone contrast at half maximum response (%)
Opn1mw^R
rd1 Opn1mw^R

A

Opn1mw^{R}

	Irradiance (Photons/cm^{-2} / s^{-1})				
	S-Cone	**Mel**	**Rod**	**L-Cone**	**Total**
Background	2.5E+11	1.6E+12	3.6E+12	1.3E+13	1.5E+13
Bar	7.9E+11	5.2E+12	7.5E+12	3.7E+13	1.1E+14
Contrast	51%	51%	34%	47%	

B

rd^{1} *Opn1mw*^{R}

	Irradiance (Photons/cm^{-2} / s^{-1})				
	S-Cone	**Mel**	**Rod**	**L-Cone**	**Total**
Background	6.0E+11	2.0E+12	N/A	1.7E+13	7.9E+13
Bar	3.9E+12	4.4E+13	N/A	9.0E+13	2.5E+14
Contrast	73%	91%	N/A	67%	

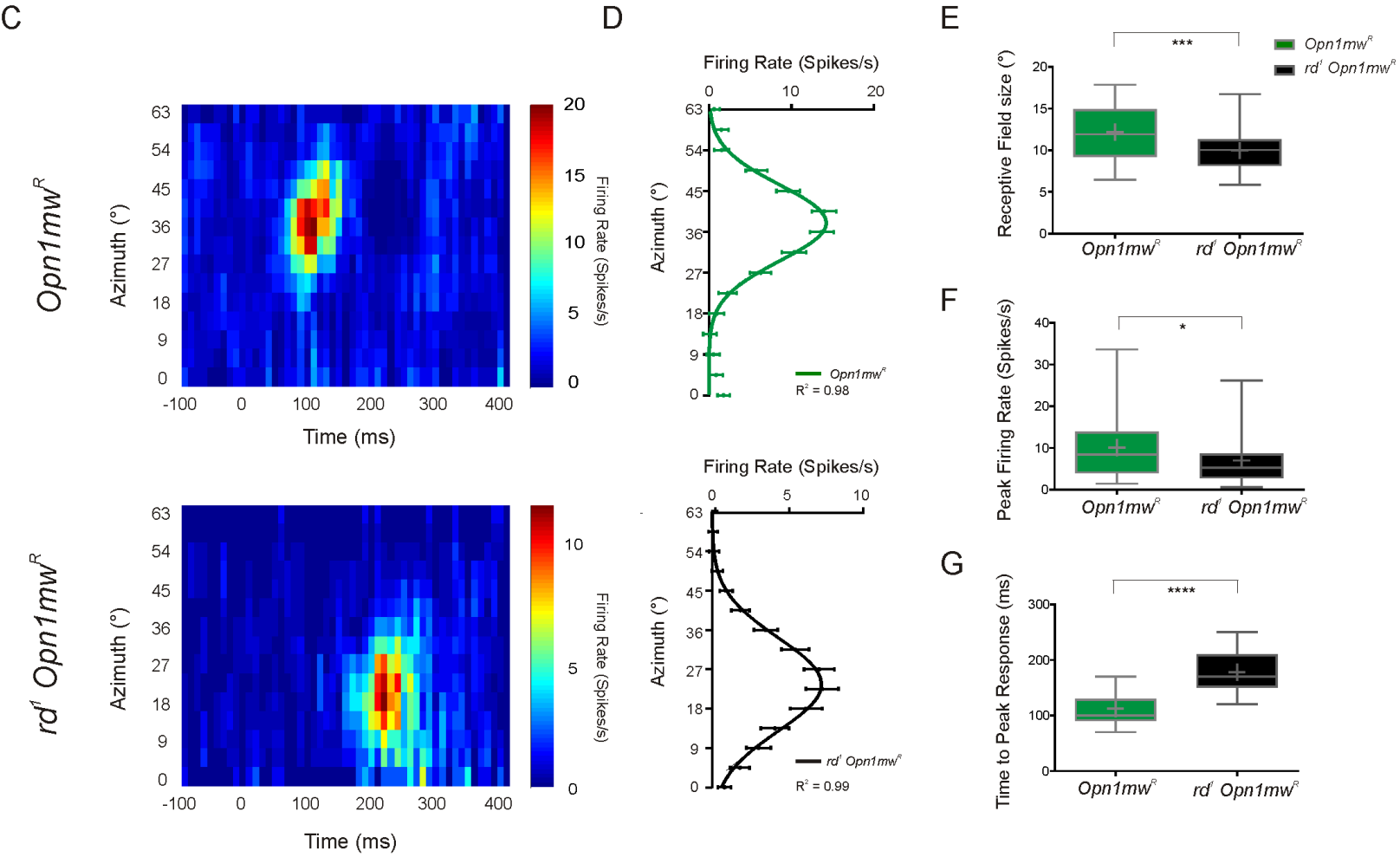

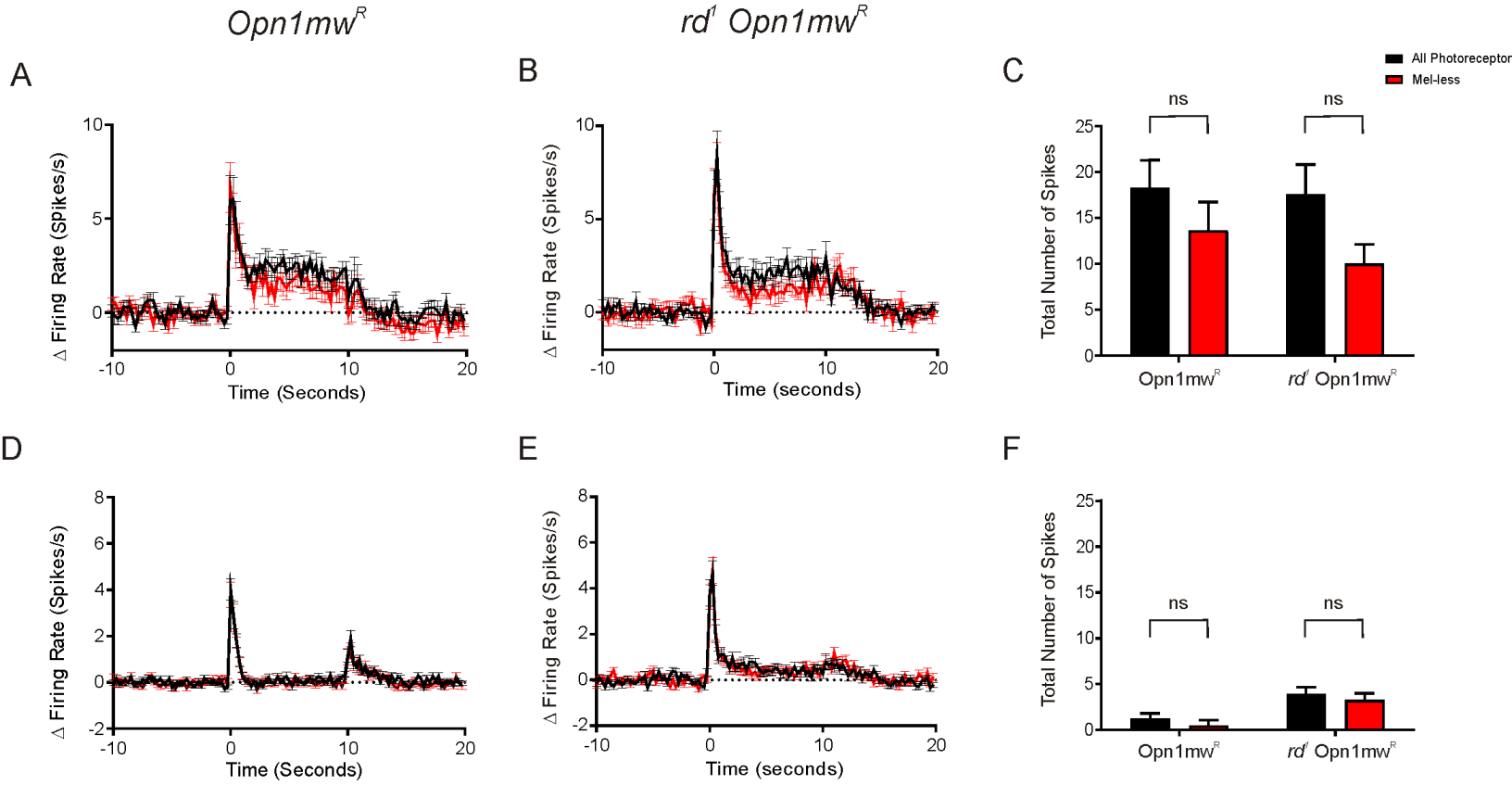
Opn1mw^R
rd1 Opn1mw^R
A
B
C
D
E
F
Δ Firing Rate (Spikes/s)
Time (Seconds)
Time (seconds)
Total Number of Spikes
All Photoreceptor
Mel-less
ns
Opn1mw^R
rd1 Opn1mw^R